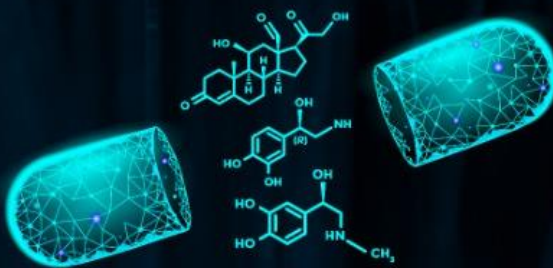


CYBER AIDD

WEEKLY REPORT



CyberAnalysis of the molecular design and optimization of the SIK2/3 inhibitor

GLPG3970 developed by Galapagos

Salt-inducible kinases (SIKs) have three subtypes, SIK1, SIK2, and SIK3, and belong to the adenosine monophosphate-activated protein kinase (AMPK) family of serine/threonine kinases. They are ubiquitously expressed in humans. Under normal circumstances, SIK1 responds to high salt or adrenocorticotrophic hormone stimulation to regulate adrenal cortical function, SIK2 participates in cell metabolism, controls insulin signaling and gluconeogenesis, and SIK3 coordinates with the mTOR complex to promote cancer. SIK inhibition represents a new therapeutic approach to regulate proinflammatory and immunomodulatory pathways and has the potential to treat inflammatory diseases. Galapagos disclosed the discovery and optimization process of the SIK2/3 dual inhibitor GLPG3970. Through high-throughput screening and structure-activity relationship studies, researchers discovered the SIK2/3 dual inhibitor GLPG3970 (compound 32), which has SIK1 selectivity and improved CYP time-dependent inhibition properties. This article sorts out the design strategy and optimization route of compound 32 (GLPG3970), which can provide valuable experience for the structural optimization of similar projects.

Pharmacodia CyberSAR system provides in-depth analysis of SIK2 target molecules. The system displays active molecules related to the target through clustered structure views and original structure views, and presents potential hits in the form of a timeline during the R&D stage. In addition, CyberSAR also provides visual analysis of indications and experimental designs to help R&D personnel quickly obtain target structure information and open up research ideas. Although CyberSAR has not been used in the initial development of molecules, it shows great application potential in analyzing and optimizing drug molecules.

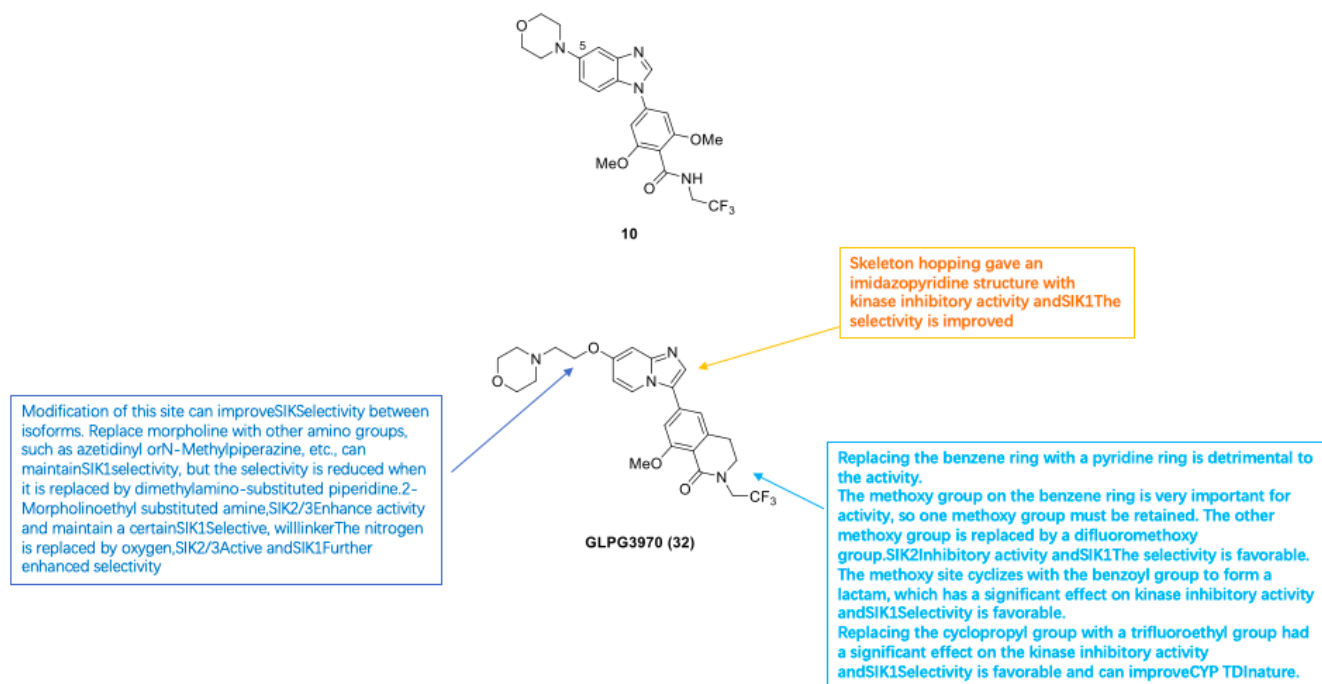


Fig1. Optimization process of compound 32 (GLPG3970)

Discovery of Clinical Candidate GLPG3970: A Potent and Selective Dual SIK2/SIK3 Inhibitor for the Treatment of Autoimmune and Inflammatory Diseases

Christophe Peixoto*, Agnes Joncour, Taoués Temal-Laib, Amynata Tirera, Aurélie Dos Santos, Hélène Jary, Denis Bucher, Wendy Laenen, Anna Pereira Fernandes, Stephanie Lavazais, Carole Delachaume, Didier Merciris, Corinne Saccomani, Michael Drennan, Miriam López-Ramos, Emanuelle Wakselman, Sonia Dupont, Monica Borgonovi, Carlos Roca Magadan, Alain Monjardet, Reginald Brys, Steve De Vos, Martin Andrews, Juan-Miguel Jimenez, David Amantini, and Nicolas Desrois*

Open PDF

Supporting Information (2)



Get e-Alerts

Salt-inducible kinases (SIKs) SIK1, SIK2, and SIK3 are serine/threonine kinases that constitute a subfamily of the AMP-activated protein kinase (AMPK) family of protein kinases. Inhibition of SIKs in stimulated innate immune cells and mouse models is associated with a dual mechanism of action, including a reduction in proinflammatory cytokines and an increase in immunomodulatory cytokine production, suggesting its potential for treating inflammatory diseases.

SIKs control the regulation of macrophage polarization. Pharmacological inhibition of SIKs can induce a macrophage phenotype characterized by the secretion of high levels of anti-inflammatory cytokines such as interleukin-10 and very low levels of pro-inflammatory cytokines such as TNF α . The researchers found that inhibition of SIK2 and SIK3 during macrophage differentiation greatly enhanced IL-10 production compared with inhibition in mature macrophages, highlighting the indispensable role of SIK2 and SIK3 in innate immunity.

Recently, JMC reported that Galapagos discovered a SIK2/3 dual inhibitor GLPG3970 (compound 32) with SIK1 selectivity through high-throughput screening and structure-activity relationship studies, which improved the CYP time-dependent inhibition properties and was effective in regulating pro-inflammatory

cytokines. TNF α Dual activity with respect to the immunomodulatory cytokine IL-10 was demonstrated in vitro in human primary bone marrow cells and human whole blood and in vivo in mice stimulated with lipopolysaccharide, and showed dose-dependent activity in disease-relevant mouse pharmacological models. The design and optimization process is summarized as follows:

Hit Discovery:

Compared with SIK full inhibitors, SIK2/3 dual inhibitors can achieve better safety and reduce cardiovascular side effects by improving the selectivity for SIK1 while maintaining ideal activity on the immune system. There have been some reports of SIK kinase inhibitors in the literature, such as Fig. 2 and Table 1, but improving the selectivity for other kinases and SIK isoforms becomes the key to developing new SIK inhibitors.

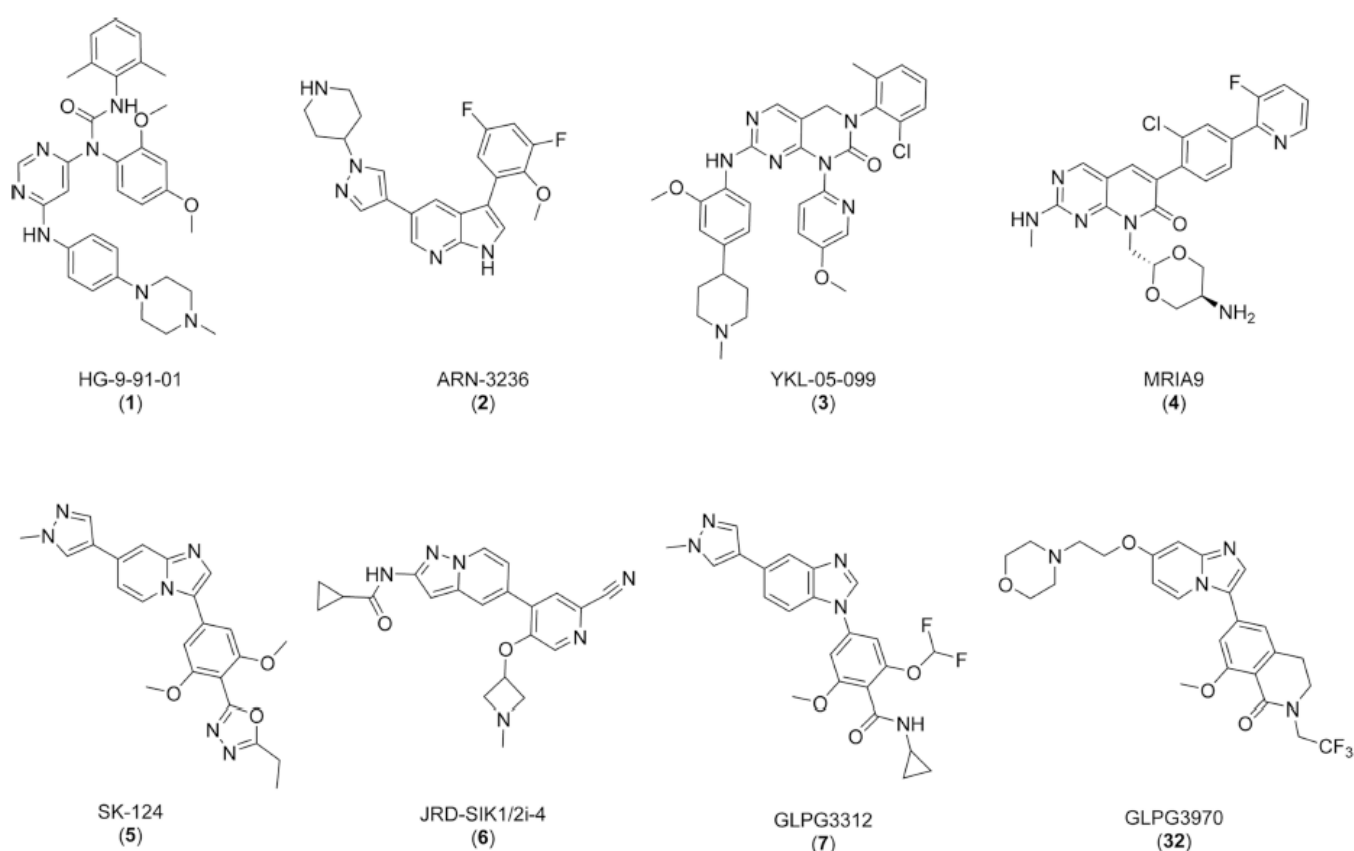


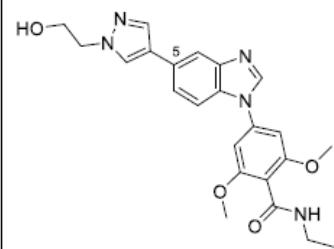
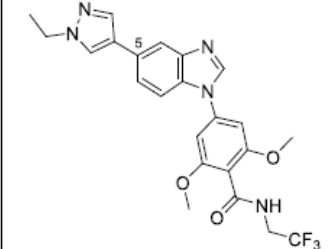
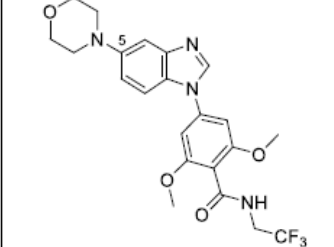
Figure 2. Structures of selected small-molecule SIK inhibitors described in the literature and of GLPG3970 (32).^{4,5,14–20}

Table 1. Reported SIK Inhibitory Activity of Compounds from Figure 2

Compound	IC ₅₀ or K _i , nM		
	SIK1	SIK2	SIK3
HG-9-91-01 (1) ¹⁵	250	67	430
ARN-3236 (2) ^{5,16,17}	21.6	<1	6.6
YKL-05-099 (3) ⁴	10	40	30
MR1A9 (4) ¹⁸	55	48	22
SK-124 (5) ¹⁹	6.5	0.4	1.2
JRD-SIK1/2i-4 (6) ²⁰	3.1	1.9	70
GLPG3312 (7) ¹⁴	2.0	0.7	0.6
GLPG3970 (32)	282.8	7.8	3.8

Through high-throughput screening, the researchers discovered that the 4-(5-substituted benzimidazole)benzoyl structure has SIK kinase inhibitory activity and obtained the co-crystal structure of compound 8 and SIK3.

Table 2. Compounds in Cocrystal Structure and Early Structure–Activity Relationship

Compound	Structure	IC ₅₀ , nM		
		SIK1	SIK2	SIK3
8		21.6	14.6	4.2
9		10.8	3.3	1.4
10		490	116.8	34.4

Sequence analysis of the three subtypes of SIK showed that there was a high degree of similarity between the three subtypes, with only five non-conserved amino acid residues in the ATP binding site. The researchers used molecular simulation to predict the effects of different residues on SIK selectivity.

sp Q9Y2K2 SIK3_HUMAN	MAAAAASGAGGAAGAGTGGAGPAGRLPPAPGSPAAPAAVSPAAGQPRPPAPASRGMP	60
sp Q9H0K1 SIK2_HUMAN	-----MVMADGPRHLORGP	14
sp P57059 SIK1_HUMAN	-----MVIMSEFSADPAGQGQQQKP	21
	*	
sp Q9Y2K2 SIK3_HUMAN	ARIGYYEIDRTIGKGNFAVVVKRATHLVTKAKVAIKIIDKTQLDEENLKKIFREVQIMKML	120
sp Q9H0K1 SIK2_HUMAN	VRVGFYDIEGTLGKGNFAVVVKLGRHRITKTEVAIKIIDKSQLDAPVNLEKIYREVQIMKML	74
sp P57059 SIK1_HUMAN	LRVGFYDIERTLGKGNFAVVVKLARHRVTKTQVAIKIIDKTRLDSSNLEKIYREVQIMKLL	81
	*:****: * :***** . * :*:*****:*** ** :*:****:***:	
sp Q9Y2K2 SIK3_HUMAN	CHPHIIRLYQVMETERMIYLVTEYASGGEIFDHLVAHGRMAEKEARRKFKQIVTAVYFCH	180
sp Q9H0K1 SIK2_HUMAN	DHPHIKLYQVMETKSMPLYLVTEYAKNGEIFDYLANHGRLNESEARRKFWQILSAVDYCH	134
sp P57059 SIK1_HUMAN	NHPHIKLYQVMETKDMLYIVTEFAKNGEMFDYLTSGHLSENEARRKFWQILSAVEYCH	141
	*****:*****: * :*:***:*. ** :*:*. :*: * :***:*** ** :*:** :**	
sp Q9Y2K2 SIK3_HUMAN	CRNIVHRDLKAENLLLDANLNKIADDFGFSNLFTPGQLLKTWCGSPPYAAPELFEGKEYD	240
sp Q9H0K1 SIK2_HUMAN	GRKIVHRDLKAENLLLDNMMNIKIADDFGFGNFFKSGELLATWCGSPPYAAPEVFEGQQYE	194
sp P57059 SIK1_HUMAN	DHHIVHRDLKTEENLLLDGNMDIKLADDFGFGNFKSGEPLSTWCGSPPYAAPEVFEGKEYE	201
	::*****:***** * :*:***:***:.. * : * *****:*****:***:	
sp Q9Y2K2 SIK3_HUMAN	GPKVDIWSLGVVLYVLVCGALPFDGPTLQNLRARVLSGKFRIFFFMSTECEHLIRHMLVL	300
sp Q9H0K1 SIK2_HUMAN	GPQLDIWSMGVVLYVLVCGALPFDGPTLPILRQRVLEGRFRIPFYFMSDCEHLIRMLVL	254
sp P57059 SIK1_HUMAN	GPQLDIWSLGVVLYVLVCGSLPFDGPNLPTLRQRVLEGRFRIFFFMSQDCESLIRMLVV	261
	** :*****:*****:***** . * ** ** :*:***:*** :** ** :***:	
sp Q9Y2K2 SIK3_HUMAN	DPNKRLSMEQICKHKW	316
sp Q9H0K1 SIK2_HUMAN	DPSKRLTIAQIKEHKW	270
sp P57059 SIK1_HUMAN	DPARRITIAQIRQHRW	277
	** :*:***: * :**:	

Figure 3. Sequence alignment between the kinase domain of SIK3 (top), SIK2 (middle), and SIK1 (bottom). The residues that form the different binding site regions are highlighted in different colors: P-loop in green, catalytic center in orange, hinge in red, bottom part in blue, and DFG motif in yellow. Additionally, non-conserved residues in these regions are indicated in black bold, showing the high similarity between the binding sites of isoforms.

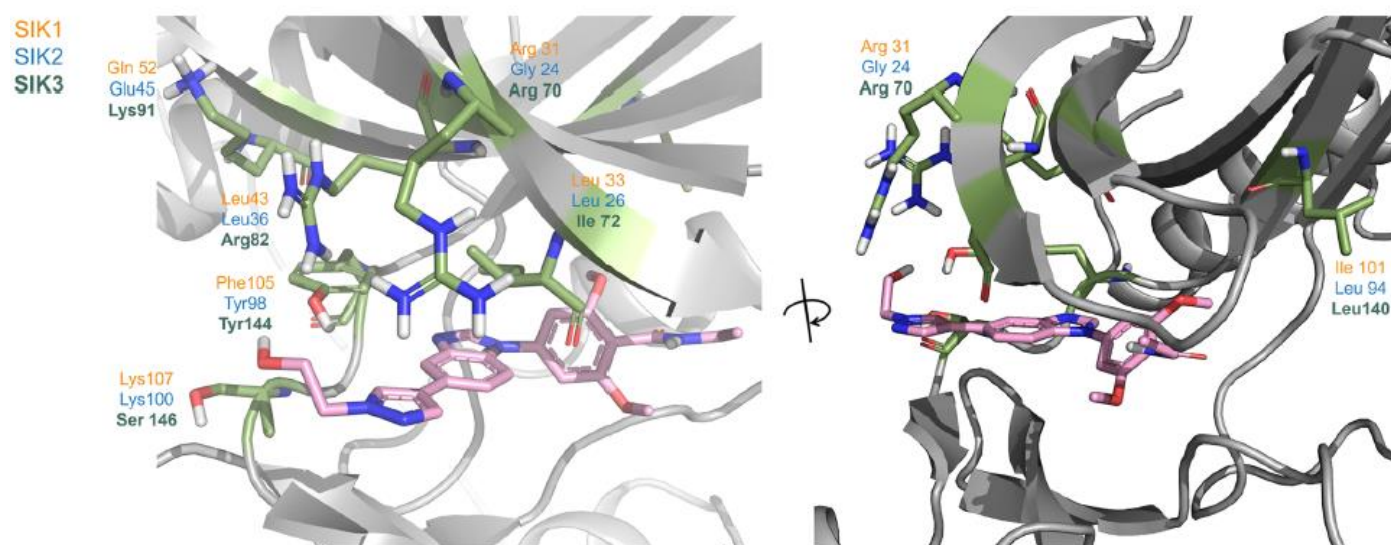


Figure 4. X-ray structure of SIK3 in complex with 8 (PDB: 8OKU). Non-conserved residues between SIK1, SIK2, and SIK3 that are located close to the binding site are displayed in sticks.

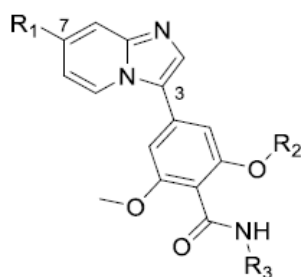
Previous structure-activity relationship studies have shown that alky pyridine The methoxy groups on the azole and benzene rings are crucial for maintaining high SIK activity. The amino acid residues near the dimethoxybenzamide group of compound 8 are very similar in different isoforms. Pyrazole The surrounding amino acid residues differ between SIK isoforms. Therefore, the researchers hypothesized that introducing different substituents at the 5-position of benzimidazole would improve selectivity for SIK1. Pyrazole Compound 10 was obtained by replacing it with the non-aromatic group morpholine. Although the SIK inhibitory activity was reduced by 25 times, it showed a certain selectivity for SIK1 and was further developed and optimized as a Hit compound.

SARexplore:

Based on the structure of compound 10, the researchers optimized the structure by skeleton transition, replacement of the morpholine functional group and modification of the benzamide group to improve the inhibitory activity of SIK and the selectivity of SIK1.

Among them, compound 10 obtained the imidazopyridine compound 11 through skeleton transition, and the inhibitory activity of SIK2/3 and the selectivity of SIK1 were improved. The structure of the bottom of the molecule was optimized, and one of the methoxy groups was replaced by difluoromethoxy, and the trifluoroethyl was replaced by cyclopropyl to obtain compound 12, which further improved the activity against SIK2 and SIK1. The morpholine of compounds 11 and 12 was replaced by other amino groups, such as difluoroazetidiny and N-methylpiperazine, showing enhanced SIK2 inhibitory activity. The activity was better after the bottom of the molecule was transformed into difluoromethoxy and cyclopropyl substitutions. However, compound 16 was terminated due to positive results in the CYP TDI test.

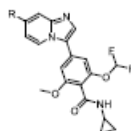
Table 3. Matched Pairs SAR on Bottom Part^a



Compound	R ₁	R ₂	R ₃	IC ₅₀ , nM			CYP TDI
				SIK1	SIK2	SIK3	
11		Me	-CH ₂ -CF ₃	314	56.8	4.7	ND
12		CHF ₂	Cyclopropyl	63.1	15.8	6.0	ND
13		Me	-CH ₂ -CF ₃	169.2	22.7	3.2	Yes
14		CHF ₂	Cyclopropyl	27.0	5.7	1.7	ND
15		Me	-CH ₂ -CF ₃	699.8	35.5	10.9	ND
16		CHF ₂	Cyclopropyl	82.5	5.4	3.1	Yes

^aAbbreviations: ND, not determined; TDI, time-dependent inhibition.

The methyl group on the piperazine ring of compound 16 was replaced by acetyl (17) and hydroxyethyl (18), and the kinase inhibitory activity was comparable. When the amine was replaced by a dimethylamino-substituted piperidine, the SIK2/3 inhibitory activity was maintained, but the SIK1 selectivity was reduced. When the piperidine was replaced by an azetidine, the SIK1 selectivity was maintained, indicating that this site was crucial for SIK1 selectivity. For example, compounds 21 and 22 did not show SIK1 selectivity, while compounds 23 and 24 were able to maintain SIK1 selectivity, but SIK2 activity was reduced.

Table 4. SAR Exploration in Position 7 of the Imidazo[1,2-*a*]pyridine Scaffold^a

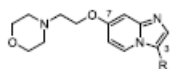
Compound	R	IC ₅₀ , nM			CYP TDI
		SIK1	SIK2	SIK3	
17		44,9	5,9	1,4	ND
18		61,1	5,3	1,9	ND
19		16,8	2,6	1,7	ND
20		112,9	10,1	4,4	Yes
21		10,0	26,4	11,5	ND
22		38,6	32,3	24,6	ND
23		240,2	48,3	3,6	ND
24		183,7	54,8	14,1	ND
25		79,7	14,1	4,2	Yes
26		51,5	4,8	1,7	No
27		6,1	1,6	0,6	Yes

^aAbbreviations: ND, not determined; TDI, time-dependent inhibition.

Replacing the amino substituent with a 2-morpholinoethyl substituted amino group can show strong SIK2/3 activity and certain SIK1 selectivity. Compound 26 obtained by replacing the nitrogen atom in the linker with oxygen shows nanomolar SIK2/3 inhibitory activity and 10-fold/30-fold SIK1 selectivity. If morpholine is replaced with tetrahydrofuran, the SIK1 selectivity is reduced.

Considering the performance of compounds 25, 26 and 27 in the CYP TDI test, the researchers modified the benzamide group based on the structure of compound 26. Replacing the benzene ring with a pyridine ring (compounds 28-30) was not conducive to activity, and the meta position of the benzene ring of compound 26 was annulated with an amide to form a cyclic lactam to obtain compound 31, which has good kinase inhibitory activity and SIK1 selectivity, while the cyclopropyl group of compound 31 was replaced by a trifluoroethyl group to obtain compound 32 (GLPG3920), which showed nanomolar SIK2/3 inhibitory activity and 36-fold/74-fold SIK1 selectivity, and was negative in the CYP TDI test.

Table 5. Bottom Part Exploration with Ether Substitution in Position 7 of the Imidazo[1,2-a]pyridine Scaffold



Compound	R	IC ₅₀ , nM			CLogP
		SIK1	SIK2	SIK3	
28		>2,633	155.9	58.2	3.1
29		866.7	113.8	56.8	3.6
30		>3,763	240.8	116.4	3.4
31		1,639	52.2	11.7	3.3
32		282.8	7.8	3.8	3.6

Combined with the results of molecular simulation, compound 32 binds to the ATP site, similar to the active conformation of compound 8, and can be classified as a type 1 kinase inhibitor. The morpholine ring of compound 32 forms a hydrogen bond interaction with Tyr144, which does not exist in SIK1, explaining the reason for the selectivity.

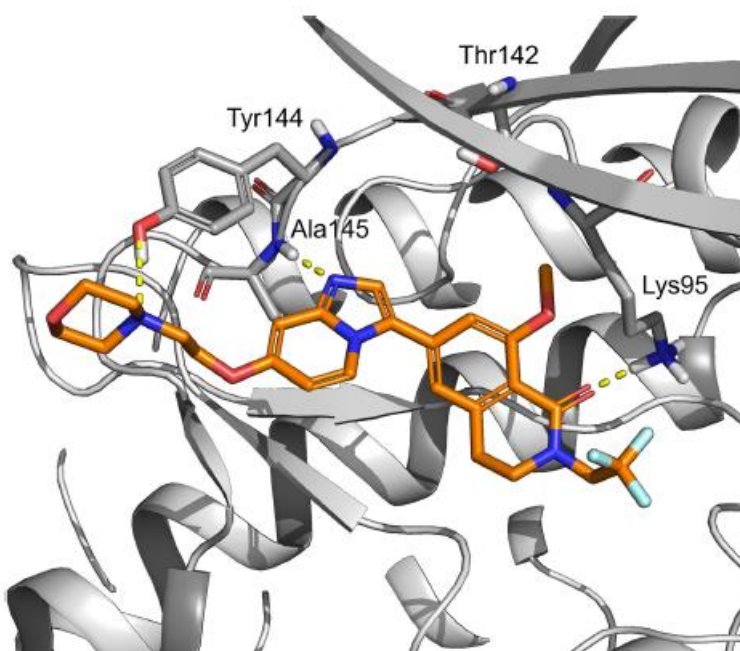


Figure S. Representative frame from molecular dynamics simulations of compound 32 (orange sticks) in SIK3 (shown in white ribbons and gray carbons). The morpholine ring is facing Tyr144, present in SIK3 and SIK2. H-bond interactions are highlighted in yellow.

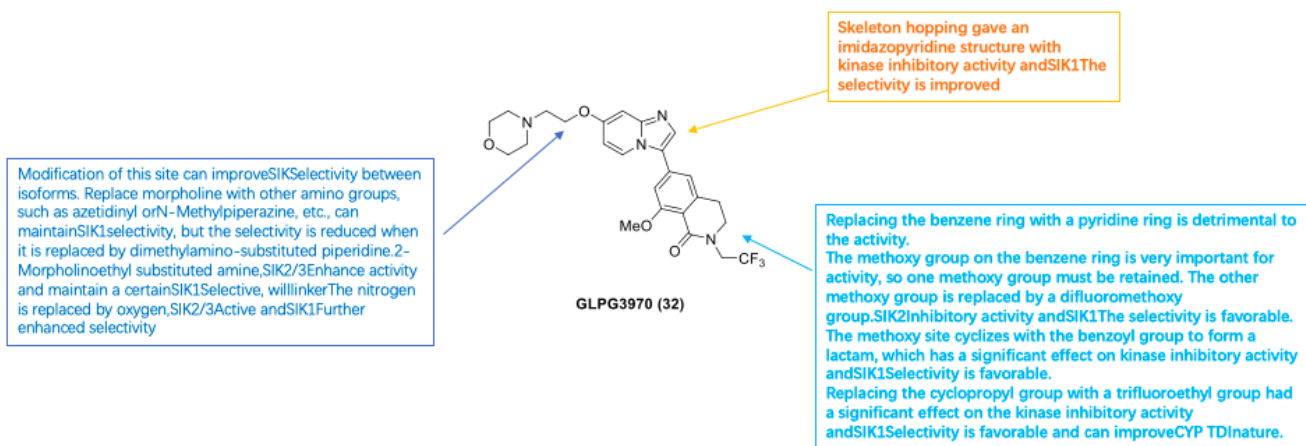


Fig6. Optimization process of compound 32 (GLPG3920)

Biological activity test:

Compound 32 was screened for enzyme inhibitory activity against 372 kinases at a drug concentration of 1 μ M. Except for SIKs, the compound only showed more than 50% inhibitory activity against 3 kinases, namely RIPK2, ABL1 and MKNK2, with IC₅₀ of 78.4nM, 1095nM, and 1074nM, respectively. It showed about 10-fold/20-fold selectivity against RIPK2. Because RIPK2 has been used as a target for drug development for inflammatory diseases, the researchers no longer considered the impact of RIPK2.

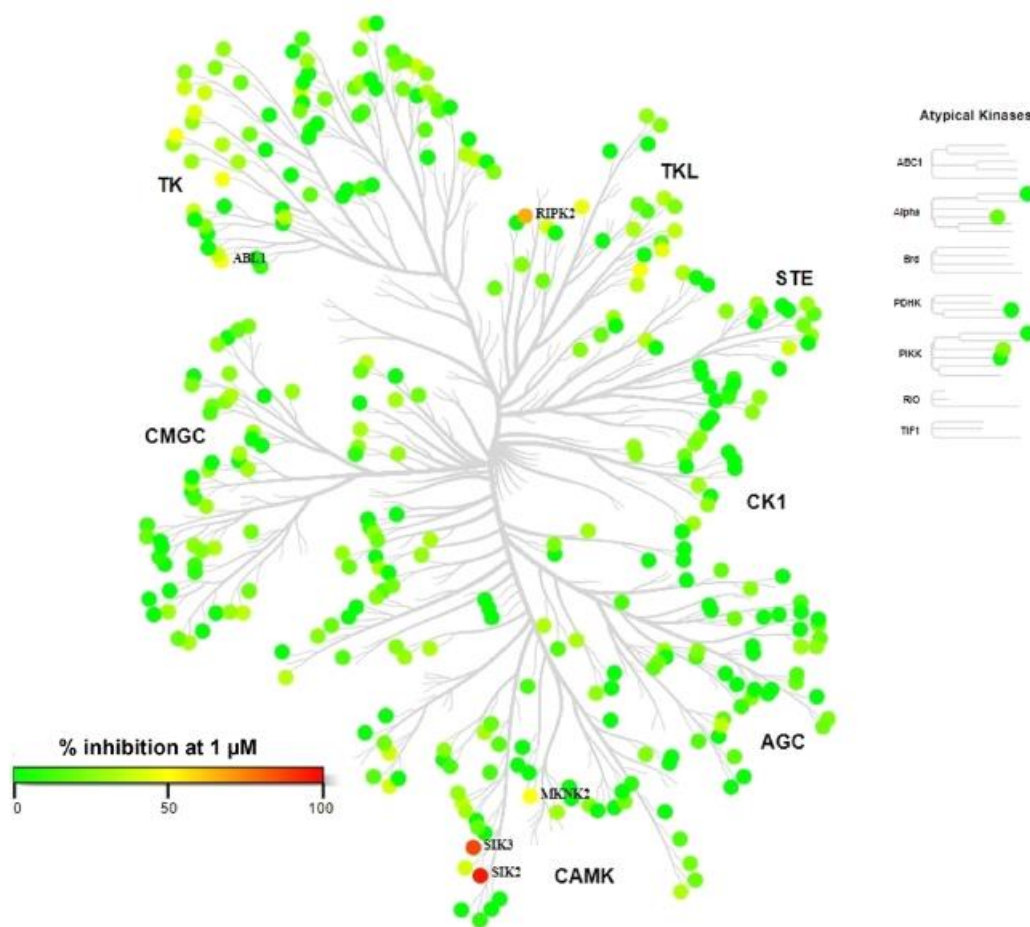


Figure 6. Kinome tree of 32 at 1 μ M.

Compound 32 showed IC₅₀ of more than 17500nM, 254nM and 79nM for SIK1/2/3, respectively, in the NanoBRET binding assay of HEK293 cells, confirming at the cellular level that the compound has potent SIK2/3 binding activity and SIK1 selectivity.

Table 6. Activity of 32 in Target-Based and Phenotypic Cellular Assays

Target-Based Cellular Assays			
Assay Model			IC ₅₀ /EC ₅₀ (nM)
NanoBRET assay (HEK293 cells)		SIK1	>17,500
		SIK2	254
		SIK3	79
CRTC3 translocation assay (U2OS cells)			1,703

Phenotypic Cellular and Whole Blood Assays			
Assay Model	Trigger/Time	Cytokine Inhibition IC ₅₀ (nM) ^a	Maximum Fold Change Increase of IL-10 ^b
Human monocytes	LPS/4 h	TNFα: 231 (5)	13.8 ± 1.9 (4)
Human monocytes	LPS/20 h	IL-12: 67 (5)	ND
Human monocyte-derived macrophages	LPS/20 h	TNFα: 365 (6)	ND
	LPS/2 h	ND	2.7 ± 0.4 (5)
Human whole blood	LPS/2 h	TNFα: 1,000 (52)	5.83 ± 0.32 (52)

^aNumber of replicates/donors for each readout indicated in parentheses. ^bCompared with LPS stimulation with no compound treatment at the same time point. Abbreviations: IL-12, interleukin-12; ND, not determined; U2OS, human bone osteosarcoma cells.

Compound 32 was able to induce the nuclear translocation of CRTC3 in U2OS cells in a dose-dependent manner with an EC₅₀ of 1703 nM. Its anti-inflammatory and immunomodulatory activities were detected using human primary myeloid cells and whole blood stimulated with LPS. In monocytes stimulated with LPS, 32 inhibited TNFα. The IC₅₀ values of IL-12 and IL-12 were 231nM and 67nM, respectively, in monocyte-derived macrophages, 32 inhibiting TNFα. The IC₅₀ of the compound was 365nM, and the production of IL-10 was promoted in a dose-dependent manner. TNFα. The IC₅₀ of inhibition was 1000nM, with a dose-dependent increase in IL-10.

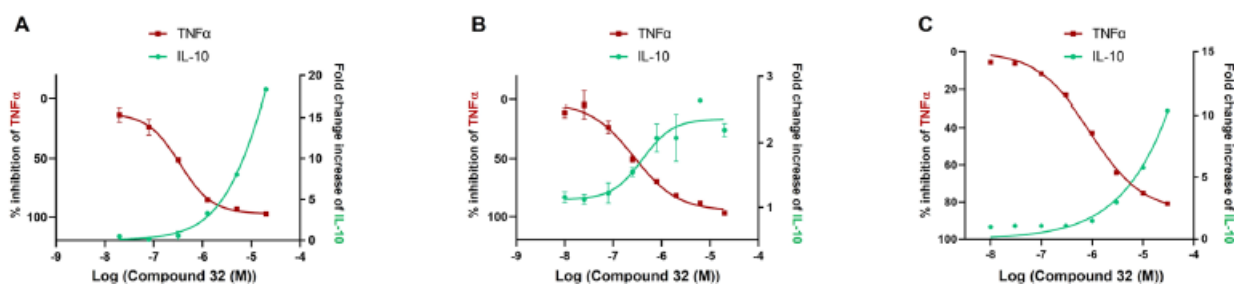


Figure 7. Representative graphs for inhibition of TNFα and induction of IL-10 by 32 in LPS-stimulated human monocytes (A), human monocyte-differentiated macrophages (B), and human whole blood (C). Data are represented as mean values of percentage of inhibition of TNFα and fold change increase of IL-10 levels. Abbreviations: IL, interleukin; LPS, lipopolysaccharide; TNFα, tumor necrosis factor alpha.

The researchers evaluated the pharmacokinetic properties of compound 32 using male mouse, rat and dog models, and administered it intravenously and orally at doses of 1 mg/kg and 5 mg/kg, respectively. In the CD1 mouse model, SD rats and beagle dogs administered intravenously after intravenous administration, compound 32 showed moderate total plasma clearance and low unbound plasma clearance, large steady-state tissue distribution, but the terminal half-life showed differences, with short, moderate and long terminal half-lives, respectively. The absolute oral bioavailability of the CD1 mouse model, SD rats and beagle dogs administered orally (5 mg/kg dose) after intravenous administration was 68.7%, 55.9% and 41.0%, respectively.

Table 7. Pharmacokinetic Properties of 32^a

	Species		
	Mouse	Rat	Dog
Strain	CD1	Sprague–Dawley	Beagle
Doses (mg/kg)	1 iv/5 po	1 iv/5 po	1 iv/5 po
CL _b (L/h/kg)	2.48 ^b	1.89 (21)	0.767 (26)
CL _u (L/h/kg) ^c	5.57	7.64	1.57
V _{ss} (L/kg)	2.51	2.82 (27)	2.89 (22)
Half-life, iv (h)	0.555	1.42 (8.1)	4.28 (11)
Half-life, po (h)	1.28 (34)	3.61 (31)	4.63 (26)
AUC _{0-∞} iv (ng·h/mL)	402	759 (21)	897 (7.0)
AUC _{0-∞} po (ng·h/mL)	1,380 (54)	2,120 (45)	1,840 (33)
F (%)	68.7	55.9	41.0

^aMean values; % coefficient of variation indicated in parentheses.
^bAssuming blood-to-plasma ratio equals 1. ^cFraction unbound in plasma is 0.445, 0.246, and 0.507 in mouse, rat, and dog, respectively.
 Abbreviations: CL_b, blood clearance; CL_u, unbound plasma clearance; V_{ss}, apparent volume of distribution at steady state.

In the *in vivo* activity test of LPS-stimulated mouse model, compound 32 showed significant effects on the cytotoxicity of 10, 30 and 60 mg/kg of 1-hydroxy-1-hydroxy-2-nitropropene. TNF α The release of IL-10 was significantly inhibited in a dose-dependent manner (>85%), with an IC₅₀ of 705nM. At the same time, compound 32 showed a dose-dependent promoting effect on the production of IL-10 (>3 times) at a dose of 3mg/kg or more.

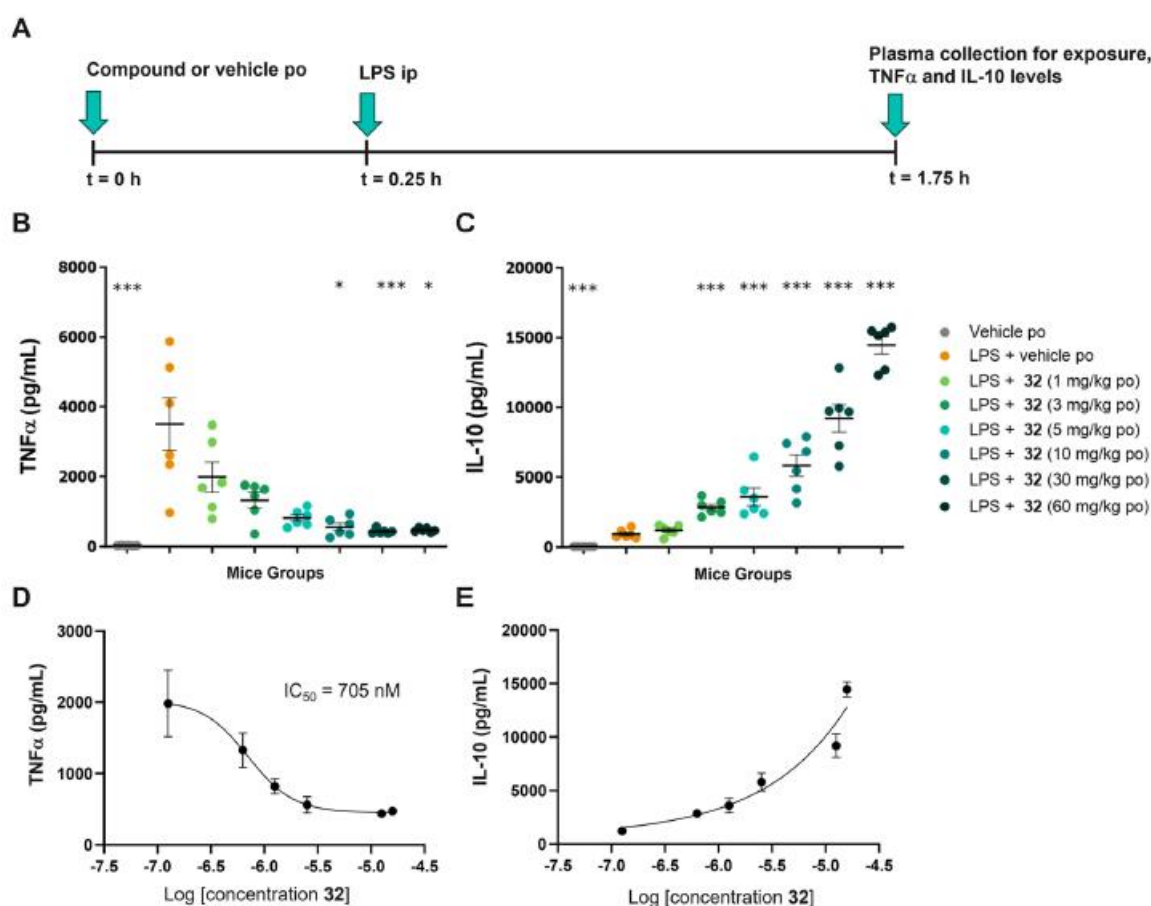


Figure 8. Plasma levels of TNF α and IL-10 after oral administration of 32 and *in vivo* LPS challenge in mice. (A) Study schematic illustrating administration of 32 ($n = 6$ mice/group) followed by administration of LPS before collecting plasma for exposure of 32 and cytokine levels. Data are presented as mean value levels of TNF α (B) and IL-10 (C) \pm SEM for each group. Statistical analysis of plasma TNF α levels versus LPS + vehicle was performed with a Kruskal–Wallis and Dunn’s post-test: * $p < 0.05$; *** $p < 0.001$. Statistical significance of plasma IL-10 levels was calculated using ANOVA and Dunnett’s multiple comparison test: *** $p < 0.001$. Exposure–response curves for TNF α (D) and IL-10 (E) are shown using mean values for concentrations (ng/mL) and cytokine levels (\pm SEM). Abbreviations: ANOVA, analysis of variance; IL-10, interleukin-10.

Table 8. Plasma Exposure of 32 and Levels of TNF α and IL-10 in LPS Challenge in Mice^a

compound 32 dose	C _{plasma} at 1.75 h (nM)	TNF α (pg/mL)	% inhibition TNF α vs LPS + vehicle	IL-10 (pg/mL)	fold-induction IL-10 vs LPS + vehicle
1 mg/kg po	129 \pm 21	1,981 \pm 426	44 \pm 12	1,217 \pm 149	1.3 \pm 0.2
3 mg/kg po	705 \pm 63	1,328 \pm 220	63 \pm 6	2,856 \pm 226	3.0 \pm 0.2
5 mg/kg po	1,216 \pm 107	821 \pm 96	77 \pm 3	3,596 \pm 628	3.8 \pm 0.7
10 mg/kg po	2,729 \pm 186	562 \pm 107	85 \pm 3	5,814 \pm 767	6.2 \pm 0.8
30 mg/kg po	13,871 \pm 1,235	438 \pm 30	88 \pm 1	9,198 \pm 997	9.8 \pm 1.1
60 mg/kg po	17,578 \pm 1,126	473 \pm 23	87 \pm 1	14,457 \pm 626	15.3 \pm 0.7

^aMean values with standard error of mean (SEM).

In the DSS-induced colitis mouse model, oral administration of compound 32 twice daily (at doses of 3, 10, and 30 mg/kg, respectively) significantly reduced the AUC of DAI scores and the histological endpoints recorded by MCHI in a dose-dependent manner. Oral administration of compound 32 twice daily (at doses of 10 and 30 mg/kg, respectively) significantly inhibited goblet cell loss, reduced inflammatory infiltration, reduced crypt density, and reduced mucosal erosion.

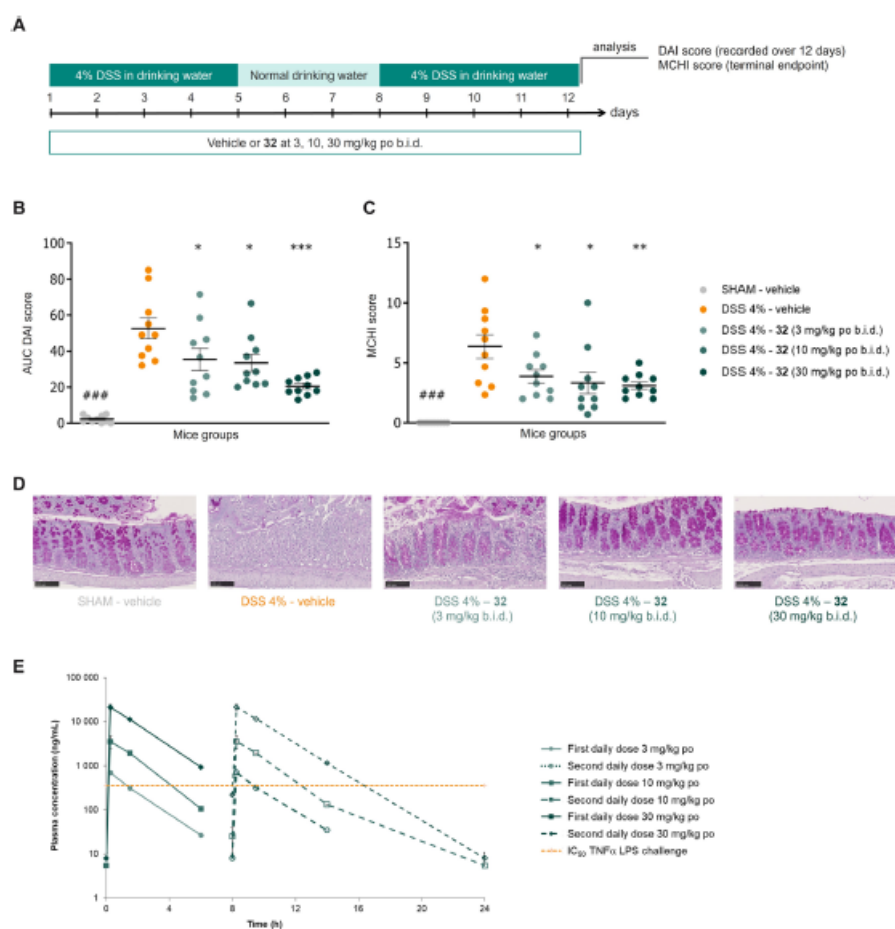


Figure 9. Activity of compound 32 in the DSS-induced colitis model. (A) Schematic setup of the mouse DSS-induced colitis model. (B) Activity of 32 on the AUC of DAI score (composite score of body weight loss, stool consistency, and fecal blood). Data are presented as mean values \pm SEM ($n = 10$ mice/group). Statistical analysis of Log(Y) AUC DAI data transformation without SHAM – vehicle group was calculated using one-way ANOVA and Dunnett's post-test analysis vs DSS 4% disease vehicle group: $^{###}p < 0.001$; $^{*}p < 0.05$; $^{**}p < 0.01$; $^{***}p < 0.001$. (C) Activity of 32 on MCHI score (mouse colitis histology index, a composite histological score of eight subscores following the published methodology).³⁵ Data are presented as mean values \pm SEM ($n = 10$ mice/group). Statistical analysis was performed with a one-way ANOVA without SHAM – vehicle group and Dunnett's post hoc multiple comparison test vs DSS 4% disease vehicle group: $^{###}p < 0.001$; $^{*}p < 0.05$; $^{**}p < 0.01$; $^{***}p < 0.001$. (D) Representative images (scale 100 μ m) of PAS-stained (and hematoxylin counter-stained) colonic tissues collected at study termination from each treatment group: "SHAM – vehicle", "DSS 4% disease – vehicle", and "DSS 4% disease – compound 32" treated with 3, 10, and 30 mg/kg (b.i.d. po). (E) Plasma exposure of compound 32 in the mouse DSS-induced colitis model on day 9 ($n = 2$ or 3 mice/time point between 0 and 6 h). The curve of the second daily dose was extrapolated and indicated by a dashed line for each group. Abbreviations: ANOVA, analysis of variance; AUC, area under the curve; DSS, dextran sulfate sodium; DAI, disease activity index; MCHI, mouse colitis histology index; PAS, periodic acid–Schiff; SEM, standard error of the mean.

In the drug interaction and in vitro safety test, compound 32 has an IC₅₀ of >33 μ M for CYP2C19 and CYP2C9 in human liver microsomes, and an IC₅₀ of >100 μ M for CYP3A4, CYP2D6 and CYP1A2. Combined with previous studies, compound 32 was negative in the CYP3A4 TDI test, and did not show obvious induction of CYP3A4 mRNA in human primary hepatocytes. The IC₅₀ for hERG ion channel was

15.3uM, and it was also negative in the in vitro genotoxicity test, indicating that compound 32 is suitable for further development as a clinical drug candidate.

Table 9 . DDI and *In Vitro* Safety Properties of 32^a

CYP450: IC ₅₀ (μM) in HLMs	>33: 2C19, 2C9 >100: 3A4, 2D6, 1A2
CYP3A4 HLM-TDI midazolam/ testosterone: IC ₅₀ (μM) initial, change (fold shift)	>33, no shift/>100, no shift
CYP3A4 mRNA induction at 10 μM in hepatocytes: fold increase vs vehicle, % increase vs rifampicin	<2-fold <20%
hERG: IC ₅₀ (μM) (manual patch clamp assay)	15.3
Genotoxicity Ames/micronucleus +/- S9	Negative/negative

^aAbbreviations: HLM, human liver microsome; TDI, time-dependent inhibition.

In conclusion:

Based on the structural differences between different SIK subtypes provided by the lead compounds and cocrystal structure information discovered earlier, the researchers optimized the structure, changed the amine substituents, enhanced SIK activity and SIK1 selectivity, and introduced an oxygen-containing linker to improve the properties of CYP TDI. At the same time, the researchers significantly improved the activity and selectivity by modifying the skeleton and cyclizing the benzamide to a lactam ring, and obtained the compound GLPG3970 (32), a potent SIK2/3 dual inhibitor that exhibits high selectivity for SIK1 and other kinases. In vitro experiments showed that compound 32 was able to inhibit TNFα. The production of IL-10 and the release of IL-10 play an immunomodulatory role, which was confirmed by in vivo LPS-stimulated mouse experiments. Compound 32 showed good effects in the DSS rat colitis model, indicating that SIK1 inhibition is not important for the immunomodulation and activity of the IBD model. In summary, compound 32 exhibits good pharmacokinetics, ADMET and in vitro safety, supporting its further development.

Source: doi.org/10.1021/acs.jmedchem.3c02246

+++++

The Pharmacodia-cyber platform integrates drug design ideas and mines active structures reported in literature and patents. Through the cyber platform, researchers can quickly and easily obtain target structures of interest to develop new ideas. SIK2 inhibitors.

Here are some examples:

1. Enter the CyberSAR homepage, in the target drop-down list, enter "SIK2", select "Associate" SIK2 Search for "Homo sapiens" SIK2 Related target information

Pharmacodia Global

Home CyberX-SAR Known SAR map CyberX-Discovery AI-driven drug discovery toolkit CyberX-Virtual Library Real-based virtual compound libraries Customized Services

Target SIK2 Target Draw Structure

Target Keyword Search "SIK2"

- SIK2 (Serine/threonine-protein kinase SIK2 | Homo sapiens)
- SIK-1 (Serine/threonine-protein kinase SIK1 | Homo sapiens)
- SIK-1 (Serine/threonine-protein kinase SIK1 | Mus musculus)
- SIK-3 (Serine/threonine-protein kinase SIK3 | Homo sapiens)
- SIP2-28 (Calcium and integrin-binding protein 1 | Homo sapiens)
- SIR2 (NAD-dependent histone deacetylase SIR2 | Saccharomyces cerevisiae S2...
- SIR2 (NAD-dependent deacetylase sirtuin 2 | Homo sapiens)
- SIR2 (NAD-dependent protein deacetylase sirtuin-2 | Rattus norvegicus)
- SIR2 (NAD-dependent protein deacetylase sirtuin-2 | Mus musculus)
- SIR2L3 (NAD-dependent deacetylase sirtuin 3 | Homo sapiens)

CyberX-SAR
Known SAR map

Target

Enhances Research Efficiency by 100x.
Customizable for ML, empowering AIDD

Create patentable chemical spaces with bioactive compounds based on Cyber AI-mined target-active molecules and proprietary datasets

AI Computation

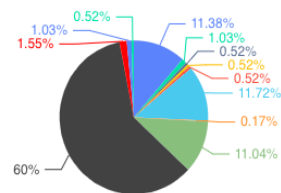
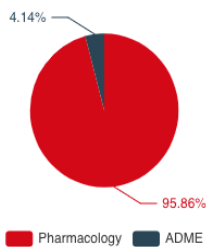
2. Select the "Experimental Data" option in the target interface to display the molecules with SIK2-related experimental test activity in the literature and patents included in the CyberSAR platform.

SIK2 : Serine/threonine-protein kinase SIK2 (Homo sapiens)

- Structure Info
- Indication
- ChemSpace
- Assay Data**
- Bioassay
- SAR Doc

Target Landscape

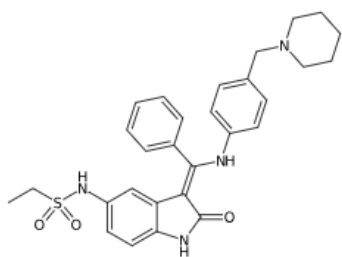
Assay Data



Assay Data 580 items

Filter Sort Default DES Page Size

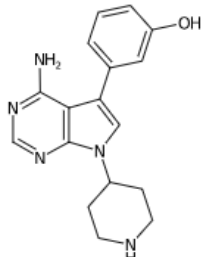
Hesperadin Preclinical



AUC = 402 ng*h/mL
mouse AUC_{0-∞}, iv (ng-h/mL) 1mg/kg

[10.1021/jm8011036](https://doi.org/10.1021/jm8011036)

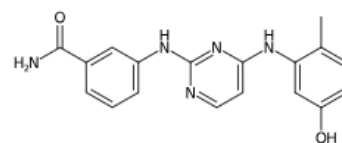
GLPG-3970 Phase 2 Clinical



AUC = 759 ng*h/mL
rat AUC_{0-∞}, iv (ng-h/mL) 1mg/kg

[10.1021/acs.jmedchem.3c02246](https://doi.org/10.1021/acs.jmedchem.3c02246)

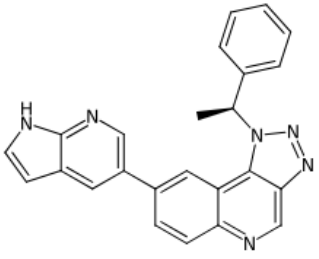
GLPG-3970 Phase 2 Clinical



AUC = 897 ng*h/mL
however, AUC_{0-∞}, iv (ng-h/mL) 1mg/kg

[10.1021/acs.jmedchem.3c02246](https://doi.org/10.1021/acs.jmedchem.3c02246)

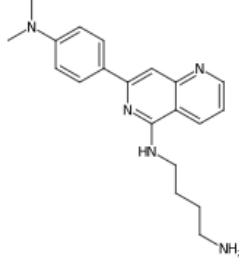
GLPG-3970 Phase 2 Clinical



AUC = 1380 ng*h/mL
mouse AUC_{0-∞}, po (ng·h/mL) 5mg/kg

[10.1021/acs.jmedchem.3c02246](https://doi.org/10.1021/acs.jmedchem.3c02246)

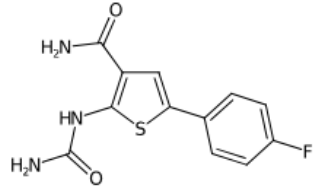
GLPG-3970 Phase 2 Clinical



AUC = 1840 ng*h/mL
dog AUC_{0-∞}, po (ng·h/mL) 5mg/kg

[10.1021/acs.jmedchem.3c02246](https://doi.org/10.1021/acs.jmedchem.3c02246)

GLPG-3970 Phase 2 Clinical



AUC = 2120 ng*h/mL
rat AUC_{0-∞}, po (ng·h/mL) 5mg/kg

[10.1021/acs.jmedchem.3c02246](https://doi.org/10.1021/acs.jmedchem.3c02246)

3. Click on the molecular structure to see further information about the molecule of interest

Pharmacodia Global 2200000004

[CYBER Pharmacodia AI](#)
[Home](#)
[CyberX-SAR Known SAR map](#)
[CyberX-Discovery AI-driven drug discovery toolkit](#)
[CyberX-Virtual Library Real-based virtual compound libraries](#)
[Customized Services](#)
中 | En

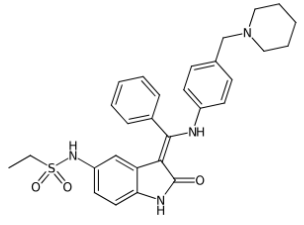
Home > Real Structure > Compound detail

Hesperadin

Structure Info

- Scaffold Similarity
- Bioisosteric Expansion
- Assay Data
- Bioassay
- Indication
- SAR Doc

Name And Taxonomy



[View Structure Chart](#) [Structure Search](#)

Name	Hesperadin
Max Phase	Preclinical
Molecular Formula	C29H32N4O3S
Synonyms	TCMDC-135395
Molecular Weight(MW)	516.67
H Donors (HBD)	3
H Acceptors (HBA)	7
LogP	5.37
Freely Rotatable Bonds (FRB)	8
Bonds (FRB)	
Polar surface area (PSA)	90.54

Property calculation based on RDKit V2022.03.3

Target

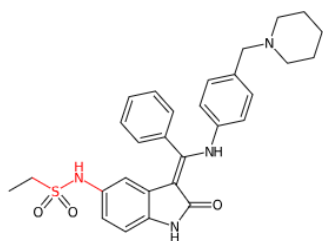
Labelled Target	
Predicted Target	AUKBA LTK ROS FAK2 MELK BRSK2 FES AURKA TYK2 AAPK1 FAK1 KS6A5 KS6A4 AURKB

Representations

SDF	Download Copy
Canonical SMILES	<chem>CCS(=O)(=O)Nc1ccc2c(c1)/C=C(/Nc1ccc(CN3CCCC3)cc1)c1ccccc1)C(=O)N2</chem> Copy
Standard InChI	<chem>InChI=1S/C29H32N4O3S/c1-2-37(35,36)32-24-15-16-26-25(19-24)27(29(34)31-26)28(22-9-5-3-6-10-22)30-23-13-11-</chem> Copy
Standard InChI Key	<chem>GLDSKRNGVVYJAB-DQSJHHFOSA-N</chem> Copy

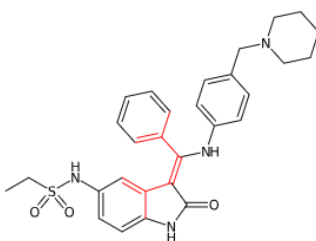
Structural Alerts

CMC Guidelines - Alert Structure Series Videos



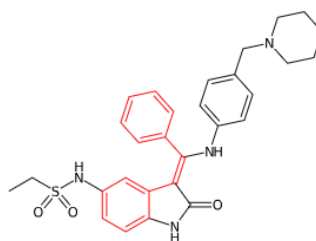
Alert Source: MLSMR

Alert Name: Hetero_hetero



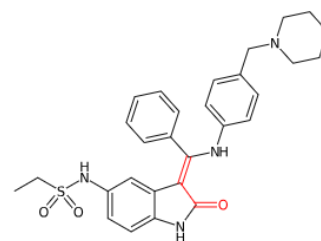
Alert Source: MLSMR

Alert Name: Dye 25



Alert Source: Dundee

Alert Name: stilbene



Alert Source: Dundee

Alert Name: Michael acceptor

4 . Clicking the "Skeleton Similarity" tab can further provide derivative types of the structure, which can be downloaded for further molecular evaluation or explore variation by chemists experience

Home

CyberX-SAR
Known SAR map

CyberX-Discovery
AI-driven drug discovery toolkit

CyberX-Virtual Library
Real-based virtual compound libraries

Customized Services

中 | En

Home > Real Structure > Compound detail

Hesperadin

Structure Info

Scaffold Similarity

Bioisosteric Expansion

Assay Data

Bioassay

Indication

SAR Doc

Real Structure

CCS(=O)(=O)Nc1ccc2c(c1)/C=C(/Nc1ccc(CN3CCCC3)cc1)c1ccccc1)C(=O)N2 [Copy](#)

Scaffold Structure

O=C1Nc2ccccc2/C1=C(/Nc1ccc(CN2CCCC2)cc1)C(=O)N2 [Copy](#)

Scaffold Similarity

Structure Similarity

Similarity : 100%

Compound Num. : 24

Similarity : 95%

Compound Num. : 36

Similarity : 94.12%

Compound Num. : 1

Similarity : 93.83%

Compound Num. : 1

Similarity : 92.86%

Compound Num. : 1

Login method

CyberSAR login URL on computer browser <https://cyber.pharmacodia.com/#/homePage>, welcome to try it out.

If you need further communication,

For a free trial, Contact us on

Anil Ranadev

+91 9742627845

anil_ranadev@saspinjara.com

Aravind

+91 9619076286

aravind.p@saspinjara.com

Sachin Marihal

+91 9538033363

sachin.marihal@saspinjara.com

Chetan S

+91 7022031061

chetans@saspinjara.com